Experimental investigation of aerodynamic interactions on a tilt-rotor configuration and comparison with Navier stokes computations

T. Lefebvre[1], C. Rondot[2], P. Sainton[2], D. Favier[2]

[1] ONERA
BP72, 29 Avenue de la Division Leclerc, 92322 Chatillon Cedex, France.
e-mail: Thierry.lefebvre@onera.fr

[2] Laboratory of Aerodynamic and Biomechanics of Motion,
USR 2164 CNRS & University of Méditerranée
163 Avenue de Luminy, 13288 Marseille cedex 09, France

Key words: Aerodynamic Interactions, Tilt-Rotor, Transition and Cruise Flight, PIV

Abstract: This paper concerns the 2nd year of the collaborative research work between LABM and ONERA research center. This work focuses on aerodynamic interactions occurring on a tilt-rotor configuration in three different flight conditions (hover, transition and cruise) [1], [2]. The present study concerns both an experimental investigation conducted in the S1L wind-tunnel at LABM combined with numerical investigations, mainly based on Navier Stokes computations (*elsA* code), done by ONERA for the same tilt-rotor and flight configurations.

INTRODUCTION

During the two previous decades, new propulsion concepts (including tilting rotors or tilting wings) have been improved in aeromechanic performance in order to decrease not only aerodynamic interactions but also acoustic and vibratory levels [3]. Nevertheless, the integration of the propulsive system and its influence on its nearest environment (wing, nacelle, airframe, etc…) still remains a restrictive factor in the optimization of this new kind of concept. Indeed, the tilt-rotor configuration is an arrangement between global handling qualities of the entire concept and aerodynamic performances of each component like rotor, wing, and airframe.
Therefore, the study of aerodynamic interactions between the rotor and its nearest environment during different flight configurations can not only be done by studying each component separately. Actually, the wing placed directly in the rotor wake influences rotor aerodynamic performance. Thus, mutual aerodynamic influences of rotor and wing are very important in different flight configurations. The interactions have already been studied for hover or low advancing speed [1], [4], [5] and [6] and in cruise [7], whereas the interactions in conversion flight are less documented and are the objective of the experimental studies of the LABM.
During 1st year of studies, several experimental methods have been developed and applied to a 1/7 tilt-rotor scale model operating in different flight configurations. Data concerning the rotor performance, the wake and the wing aerodynamic behaviour have thus been obtained for investigating the aerodynamic interactions on a tilt-rotor operating in different flight configurations.
This paper concerns the 2nd year of the collaborative research work between LABM and ONERA research center on aerodynamic interactions occurring on a tilt-rotor configuration. After a brief description of the experimental set-up , the CFD calculations performed on the cruise configuration are presented and compared to the experimental data, especially concerning the wing behaviour. Then the 2nd year experimental investigation conducted in the S1L wind-tunnel at LABM is analyzed using the PIV 3C results on cruise and conversion configurations.

1. EXPERIMENTAL SET UP

Two campaigns of experiments have been performed on a 1/7 scaled tilt-rotor model set-up in the LABM S1L wind-tunnel as shown in Figure 1. The rotor is mounted in the V1 wind-tunnel test section (3m in diameter, 6m in length, maximum velocity 100 ms^{-1}) by means of a vertical cylindrical mast which can be rotated by a shaft angle β in order to allow the simulation of the hovering flight (corresponding to β=90° in figure 1a), the conversion (corresponding to β=45° in figure 1b) and the cruise (corresponding to β=0° in figure 1c).

a) Hovering Flight, δ=50deg b) Conversion Flight, δ=50deg c) Cruise flight, δ=0deg

Figure 1: Views of the tilt-rotor set-up in different flight configurations

The set-up (Figure 2) also includes a fixed wing in the rotor wake as well as an end plane plate simulating a symmetry plane (2m*2m*0.25m). The wing is maintained in the test section by a secondary rotating mast which is mounted on the upper part of the wind-tunnel test section. The wing has a span h=0.770m, a chord c=0.31m and is equipped with an OACV23 airfoil profile.

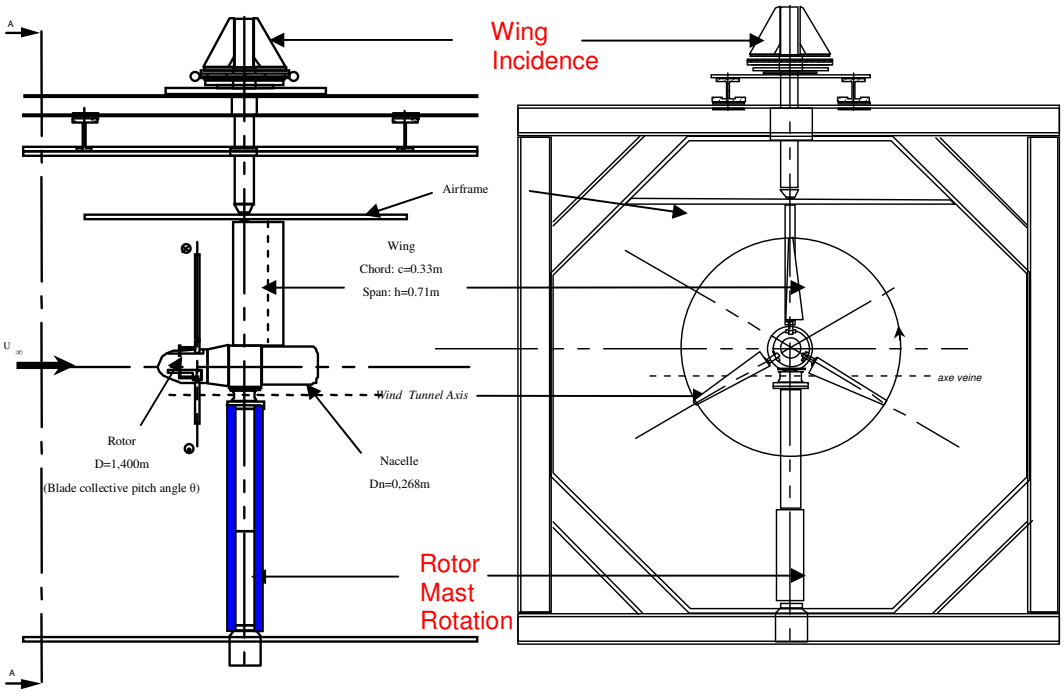

a) Front View b) Side View

Figure 2: Sketch of the tilt-rotor configuration.

The rotor (diameter D=0.140m and hub diameter D_0=0.27m) is fully articulated and equipped with a nacelle and 3 blades having non linear twist and chord laws and 3 different airfoil profiles along the blade span (OH120, OA312 and OA309). The planform of the LABM blade is shown in Figure 3 and is based upon EUROFAR blade geometry [8].

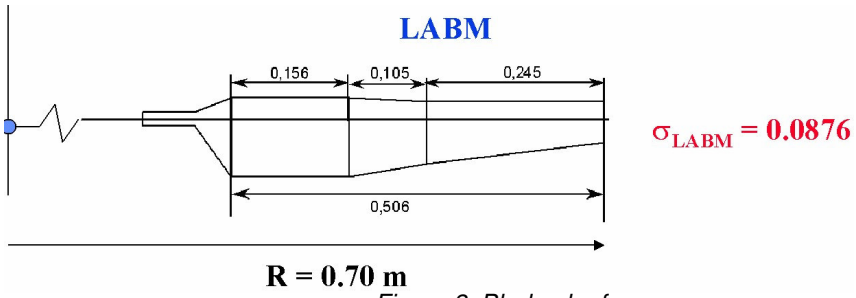

Figure 3: Blade planform

2. NAVIER STOKES COMPUTATIONS ON CRUISE CONDITONS

The first objective of the CFD calculations is to select the mesh strategy and the calculations parameters in order to reproduce the experimental behaviour of the rotor / wing interactions measured in cruise conditions during 1st year of the study. The result will determine the interest of using this numerical set-up to improve the knowledge of the physical phenomenon occurring during the aerodynamic interactions for all the transition phase of a tilt rotor.

2.1 Mesh and calculations description

2.1.1 Mesh description

The retained methodology had to fulfill two objectives:

- to take into account the experimental set-up with the best accuracy , as well as the upper and lower wind tunnel walls. It also has to consider the gap between the nacelle and the wing,
- to be easily adaptable that is to say to allow the calculation, without remeshing, of the isolated wing or the full set up. Moreover, changing the wing angle or the nacelle angle should not be a constraint for the meshing process.

Starting from LABM geometrical data, the meshing of all the parts was perfomed using ICEM HEXA. Considering the specificities of the tilt rotor, with various elements that can tilt independently (like wing and nacelle), the Chimera method [9] was retained for this study. This method allows simplifying the meshing process for complex geometries and relative moving bodies. It consists in overlapping child grids on background ones and transfers the different solutions thanks to interpolation algorithm. Actually, this method enables to integrate in a background grid, precise mesh for all single geometries. In our steady case, we have generated one mesh per element (mast, wing, nacelle, rotor) independently from the others.
Considering the rotor, on this first study, it is considered as an actuator disk [10] that represents the time average effects of the forces of the blades. Two kinds of actuator were used: the uniform one (UAD), only representing the average thrust effect and the non uniform one (NUAD), taking into account the azimuthal and radial distribution of the thrust. The main advantage of this method is to model an unsteady case with a steady calculations which leads to a gain in time and mesh size.
Eventually the final Navier Stokes mesh contains 2.3 Millions of points (for the full set up) and is presented Figure 4.

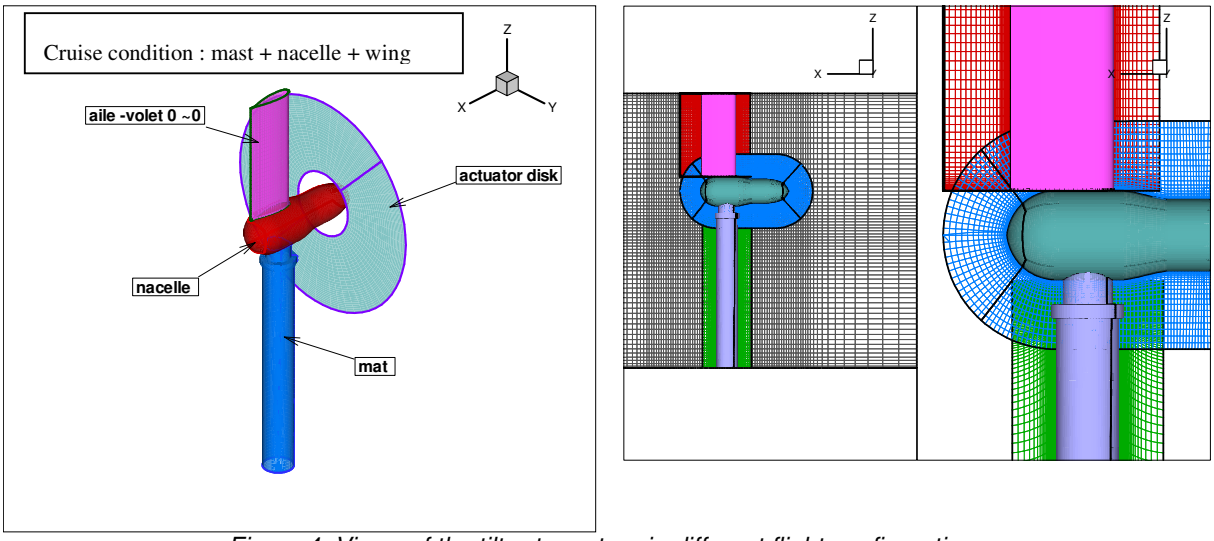

Figure 4: Views of the tilt-rotor set-up in different flight configurations

2.1.2 *elsA* code description

The *elsA* software [11] developed by ONERA, solves the Reynolds – Averaged Navier – Stokes equations in a finite volume formulation.
All the calculation performed within this study were under steady assumption (local timestep). The 2^{nd} order spatial discrimination of the conservative system is ensured by the space-centred Jameson's scheme. The 2^{nd} and 4^{th} order coefficients of the Jameson artificial viscosity are equal; respectively to 0.5 and 0.032. The time integration is done with the Backward Euler scheme and an LU scalar relaxation implicit phase. For the Navier Stokes computations the k –ω turbulence model is used with the SST correction and the Zheng limiter. The calculation does not include any transition criteria. Moreover, as the Mach number is close to 0.1, the low speed preconditioning was evaluated in order to check the effect of the accuracy of the simulation. Considering the boundary conditions, the upper and lower walls of background grid are in Euler type.
The CFD activity was divided into 3 kinds of calculations, thanks to Chimera technique, to match with the experimental measurements:

- isolated wing calculations (2D, 3D),
- wing, nacelle and mast,
- wing, nacelle, mast and rotor (actuator disk).

2.2 Isolated wing calculations

The first computations were made on the isolated wing both in 2D and 3D. The 2D calculations aimed at evaluating the wing mesh and the effect of *elsA* retained assumption of fully turbulent flow on the accuracy of the solution. We therefore extracted a 2D section of the 3D mesh of the wing (and of the background grid) to perform *elsA* 2D computations that was compared to ISES [12] calculations on the wing airfoil.
Figure 5 present the Kp distribution results for 4 calculations: ISES 2D / ISES 2D fully turbulent/ *elsA* 2D fully turbulent / section of *elsA* 3D fully turbulent (section close to the WT wall)
Up left is compared the transition effect in ISES calculations: one can easily visualize the difference especially in the leading edge area and on the transition zone. The difference on Cz is obvious, reaching around 20 % (Cz = 0.382 with transition et 0.302 without).

Up right is plotted the ISES fully turbulent and *elsA* 2D calculation. The agreement is satisfactory with a good *elsA* 2D prediction concerning the Kp levels: Cz are similar with less than 5 % of difference.
Bottom right is plotted the pressure field on the 3D wing (from *elsA* 3D calculation) with the section used for 2D / 3D *elsA* comparison, plotted on bottom left figure. The difference is visible on the Kp level with a slightly smaller Kp for 3D section.

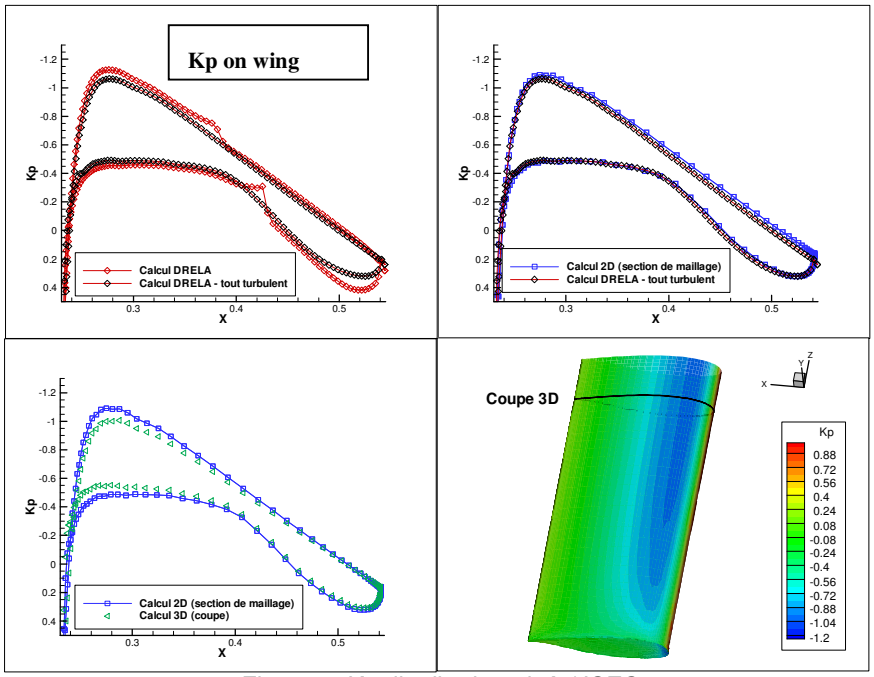

Figure 5: Kp distribution elsA / ISES

This preliminary CFD activity, comparing ISES and *elsA* calculations proved that the quality of the wing mesh is satisfactory enough to be trusted when comparing with experimental results. But it also indicates that not considering the transition influence in *elsA* calculation will lead to under estimate of the Cz in the calculation compared to the experiment.

2.3 Complete set up calculation

2.3.1 Global loads

This part of the paper will deal with the nacelle influence on the wing behaviour. Compared to the previous isolated 3D wing computation, the nacelle and the mast have been included in the calculation. Figure 6 presents the comparison, in terms of Cz and Cx function of the wing incidence, between CFD calculations and experimental data from LABM WT tests.
Considering the Cz values, even though the calculated and experimental curves are not superimposed, the slope are similar between both kind of data, either for the isolated wing or for the full setup. Moreover the wing nacelle configuration provides an higher lift than the 3D wing. The "absolute" gap between the data certainly comes from the lack of transition in the *elsA* computations (as demonstrated in preliminary ISES calculations). One has to note that the preconditioning effect as a very limited influence on the global coefficients for this test case (M = 0.135). Considering the Cx behaviour, similar behaviour can be observed with even better agreement between CFD and experiment on the Cx at 0 °.

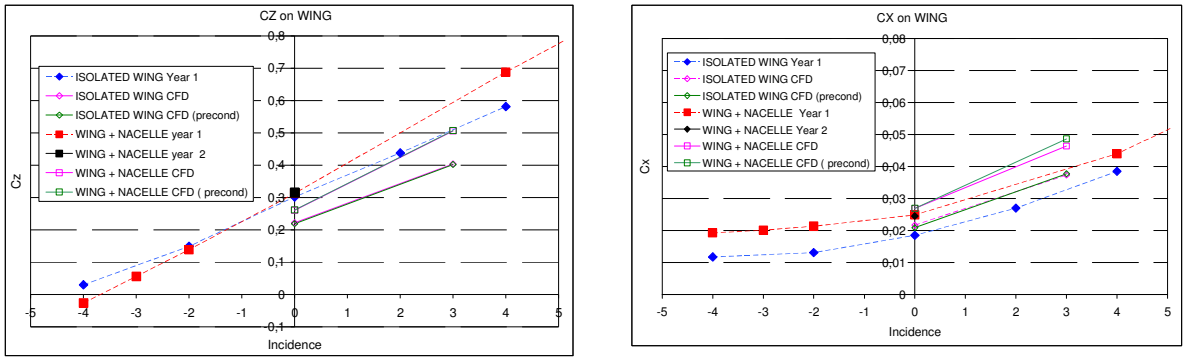

Figure 6: Comparison of wing aerodynamic data (Cz and Cx) between CFD and experiment

As stated earlier, the rotor is taken into account through the actuator disk either with uniform (UAD) or non uniform one (NUAD). Using the actuator only increased the CPU time by 10 %.
Figure 7 (left) presents the computational result with the streamlines around the nacelle, for the cruise condition with actuator disk. On Figure 7 (right) is plotted the comparison of calculated and experimental wing upload due to the rotor effect on cruise configuration. For a similar imposed thrust of 50 N, we obtained an upload of around 1% for UAD and 3.5 % for NUAD. As expected, both AD model predict a positive wing upload but with better agreement with experiment for NUAD model.
It seems clear that only including the real blades movement in the calculation would enable to increase the accuracy of the prediction but it would impose the use on unsteady calculations with an increase of CPU (and meshing).

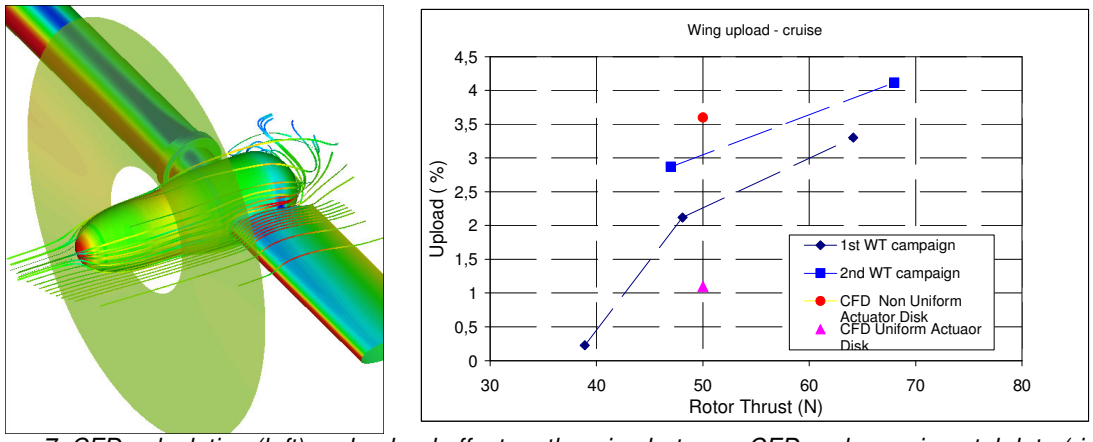

Figure 7: CFD calculation (left) and upload effect on the wing between CFD and experimental data (right)

2.3.2 Pressure analysis

Figure 8 (left) presents the Kp behaviour for sections on the wing for both isolated and with nacelle wing. Four sections are compared: the first one is located at z/R = 0.285 (not instrumented in WT tests) and 0.616, 0.716 et 1.016 (measured during WT tests). The first section shows the important influence of the nacelle on the wing tip region due to the vortex formation at the tip of the isolated wing. The Kp level of the isolated wing are closer for the other three sections but still with slight differences up to 90 % of the blade. This may be due to a small increase of the speed when adding the nacelle and mast.
Concerning the rotor influence, the same information can be found on Figure 8 (right) where the Kp distribution of the 4 sections are plotted. At this scale, the rotor influence is hard to evaluate, except

for r/R = 0.716 section. Thus a zoom effect on the Kp peak is plotted on Figure 9 (left): one can check that the most influenced section is the r/R = 0.716 one. Logically, the NUAD, that reproduces the radial distribution of blade forces, as a stronger effect in this region corresponding to the maximum blade thrust. Figure 9 (right), presents the same zoom on the experimental Kp measured during 1st year of WT tests. Even though the absolute values differ, both calculations and experiments show that the maximum influence is located in section r/R = 0.716 and that the effect is still visible at 1.016.

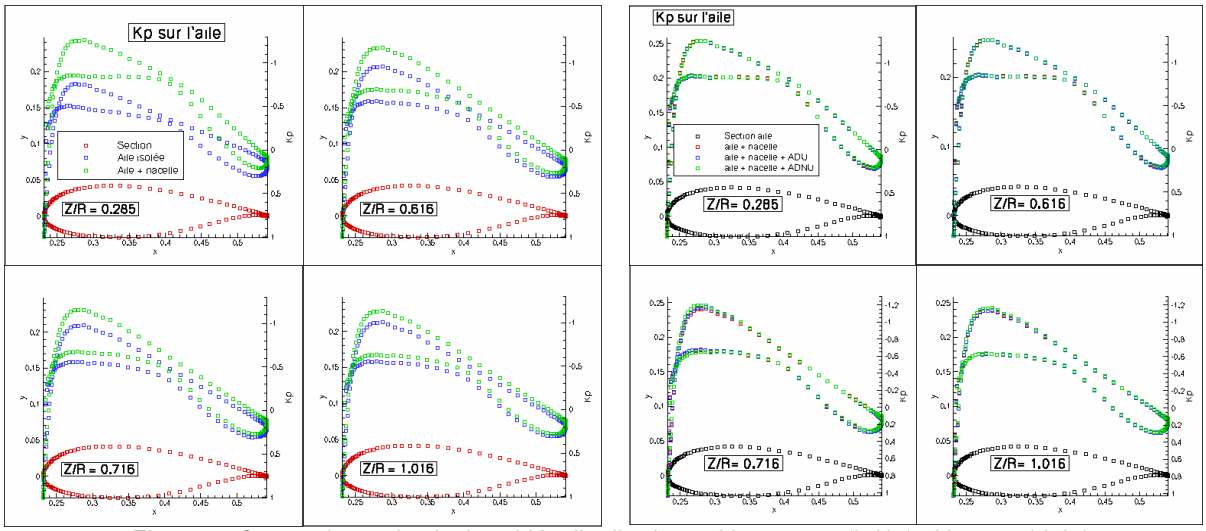

Figure 8: Comparison of calculated Kp distribution: without rotor (left) / with rotor (right)

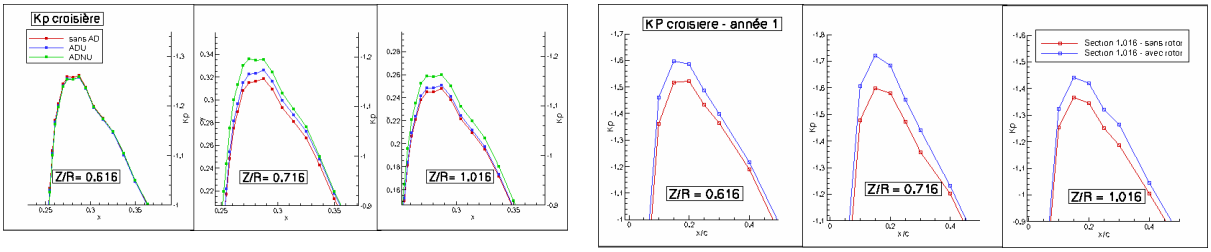

Figure 9: Zoom on the rotor influence on Kp distribution: CFD (left) / experiment (right)

2.3.3 Flow field analysis

In order to understand better the AD influence on the wing, Figure 10 presents the evolution of speed characteristics for a line located just in front of the wing leading edge, along the span. Considering the Vx speed (freestream direction), the UAD exhibits a constant increase of speed along its influenced area whereas the NUAD case has an increase more concentrated around the area of blade maximum thrust. Considering Vy (positive upwards), of low amplitude, we can notice the highest difference between the 2 AD models: UAD is close to non actuator case whereas the NUAD predict an increase of incidence on the wing around 70 – 80 % of the blade radius (rotor sense of rotation effect). Vz behaviour (span wise direction) is similar for both AD models

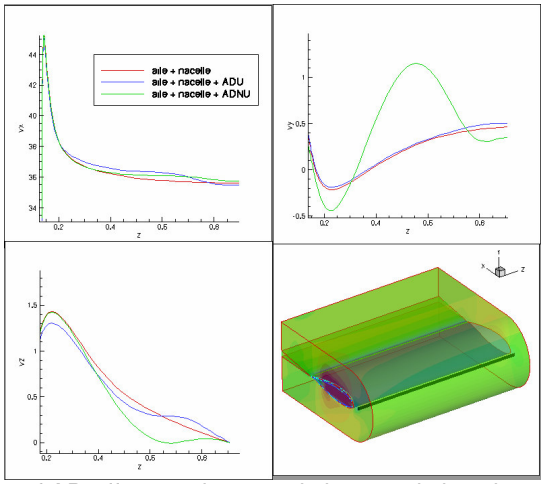

Figure 10: Comparison of AD effect on the speed characteristics along the wing leading edge

2.4 Conclusion on CFD

Considering the wing behaviour, the CFD calculations provide a good agreement with experimental results for global data (thrust and drag). Moreover, the use of actuator disk (non –uniform) enables to predict the rotor upload effect on the wing. Concerning the local pressure data, the local effect of the rotor on the various sections of the wing is in coherence with the experimental values.
Therefore, the 1st objective of the CFD calculation is achieved: the selected mesh strategy and the calculations parameters allowed to reproduce the experimental behaviour of the rotor / wing interactions measured in cruise conditions. To achieve the 2nd aim of this activity, that is to say to use the numerical set-up to improve the knowledge of the physical phenomenon occurring during the aerodynamic interactions for the transition phase, some modifications should be made to improve the quality of the calculations: it seems mandatory to integrate the transition effect on the wing and the blades should be included in the computations.

3. EXPERIMENTAL ACTIVITES

This part will mainly deal with the introduction of PIV 3C measurements in the study of tilt rotor aerodynamic interactions. The objective of using this measurement technique is to evaluate its capabilities to explore more precisely the zone of interaction between the tip vortices and the wing.

3.1 PIV set up

The 3C PIV set up use an acquisition system from DANTEC, FLOWMAP 1500. This system is linked to a computer containing the FLOWMANAGER software for data storage and post - processing. To achieve these measurements, two pulsed Nd-YAG lasers are used: they are located in the right side wall of the wind tunnel test sections for all the planes (2*150 mJ) and provide a laser sheet of about 5 mm of thickness. Two cameras (CCD 1280 x 1024 pixels) are located in the opposite wall of the test section. The laser beam and the camera recording are synchronized with the azimuthal blade positions through in incremental encoder. This encoder is based on the top signal coming from blade passage. The seeding is ensured by an oil generator (leader SMOG) located downstream the test section with particles having a calibrated diameter varying between 0,8 – 1 µm. On Figure 11 (left) are indicated the location of the various components of the PIV systems inside the WT section.

All the PIV measurements planes have been defined perpendicular to the freestream direction and are used both for cruise and conversion configurations. For these reasons, the laser sheet is generated in a plane perpendicular to the flow and can be moved from upstream to downstream parallel position. Figure 11 (right) provides a 3 D visualization of plane location in conversion. 3 PIV planes were considered a constant Z location (around z/R= 1): the aim was to characterize the rotor wake behaviour before the interaction with the wing (up to trailing edge) and after, in the wing leading edge section. Another plane was located behind wing tip to evaluate the nacelle influence.

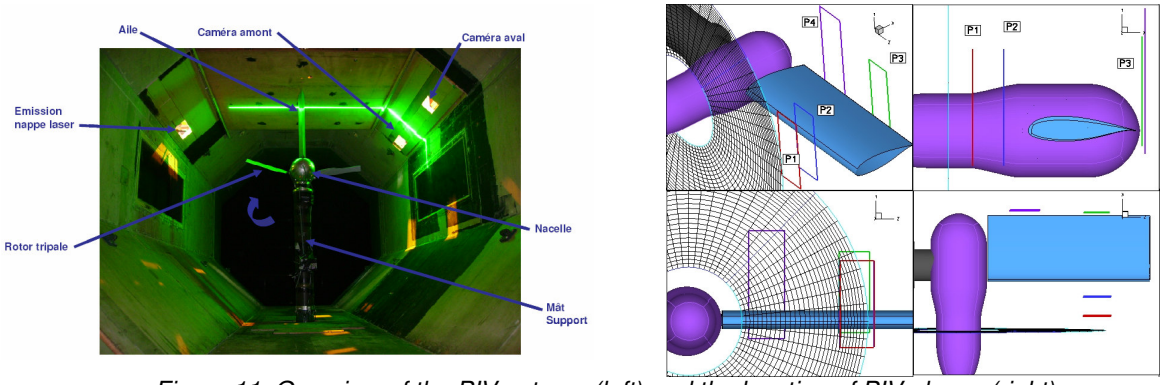

Figure 11: Overview of the PIV set –up (left) and the location of PIV planes (right)

One has to note that, at the beginning of the study, other PIV planes were expected, located above the suction side of the wing, to explore the vortex wing interactions. But as the camera and laser should have been place on the same side to WT, the expected reflection of the laser on the wing led to abandon this PIV planes for the present studies.

For each PIV plane, the PIV window is made of the rectangle of the following sizes 330 mm * 125 mm (300 perpendicular to the wing and 125 along the span of the wing) and each window contains 90 * 80 velocity vectors. Concerning the azimuthal distribution of the PIV acquisitions, 26 acquisitions per rotation were recorded as follows:

- for blade1: 24 azimuthal positions (every 5 ° of the blade rotation) : 5°/ 10°/ 15° → 115°,
- for blade 2: 1 azimuth for 120 °,
- for blade 3: 1 azimuth for 240 °.

Each final picture is the result of averaging of, at least, 100 instantaneous pictures acquisitions.

3.2 PIV results

The PIV results will be presented for the 2 most interesting planes, located along the wingspan at the expected location of tip vortex interaction in cruise conditions**:**

- the first one (called P2) is located between the rotor and the wing, thus before any interaction with the wing,
- the second one (called P3) is located after the trailing edge of the wing**.**

One should note that the 0 ° azimuth corresponds to the blade 1 in line the wingspan.

3.2.1 PIV in cruise

The cruise configuration is the most adequate one to start with PIV analysis as the wake is helicoidal and the PIV planes are equidistant from the rotor disk.

P2 plane

On Figure 12 (left) is plotted the location and intensity of the tip vortices "captured" by P2 plane in function of the blade azimuth. One can notice that the vortices are regularly disposed in function of azimuth and that they "follow" the blade rotation with a delay of 22° which represents the travel time between the rotor and the P2 plane. Another interesting point is that, knowing that the rotor disk – plane distance is constant, they should all have a similar intensity which is not he case: actually, the upper vortices present a lower intensity than the lower ones. One can suppose that the resolution of the PIV is not of the same quality everywhere in the window. On the right hand side of Figure 12 are compared the tip vortices experimental location with the theoretical ones predicted with HOST code (for isolated rotor assumptions) [13] with a side view of the nacelle and also a front view of the wing and rotor disk. One can check the good agreement of the vortices centres with the rotor disk.

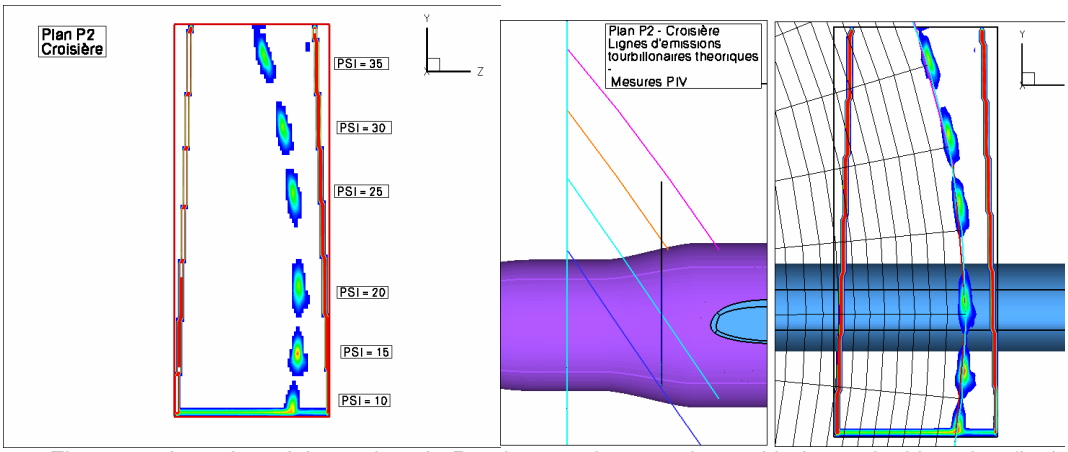

Figure 12: Location of tip vortices in P2 plane and comparison with theoretical location (isolated rotor)

The following figure (Figure 13) provides a 3D view of the intersection between the theoretical emissions lines, and the vortices centres. Some slights discrepancies can be observed possibly due to the wing proximity modify the vortices trajectories.

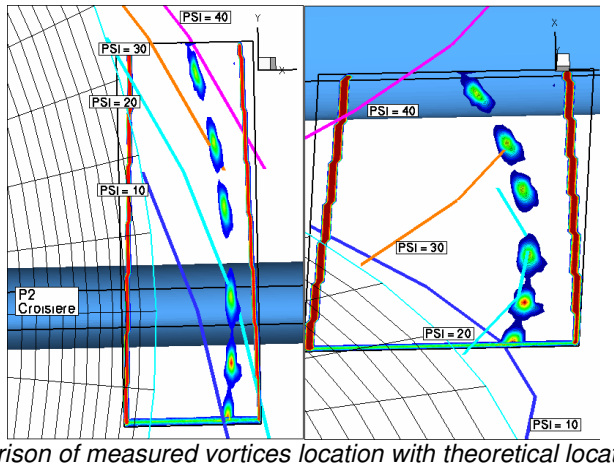

Figure 13: Comparison of measured vortices location with theoretical location

Figure 14 (right) briefly presents the 3 speed components (averaged value) for 1 azimuthal blade location. These values permit to obtain the 3 D spatial location of the tip vortex before interaction. Actually, as plotted on the left side of the Figure 14, in this cruise configuration, the collective pitch

reaches 44 ° for a –7 ° twist at blade tip, thus the blade tip has 37 ° of angle with the PIV plane. The tip vortex is therefore tilted, its rotational vector also having a 37 ° of incidence directed upwards.
Concerning W components (free stream direction), one can check that the average speed outside the wake influence reaches the expected 46 m/s and that the internal part of the tip vortices increase the speed whereas the external part reduces it. For U component (vertical speed for the wing, negative upwards), the spatial location of the vortex is confirmed with the increase of incidence in the external part of the vortex. One can note the rotor wake visualization in the PIV plane. The V component add the last piece of information for vortex spatial location.

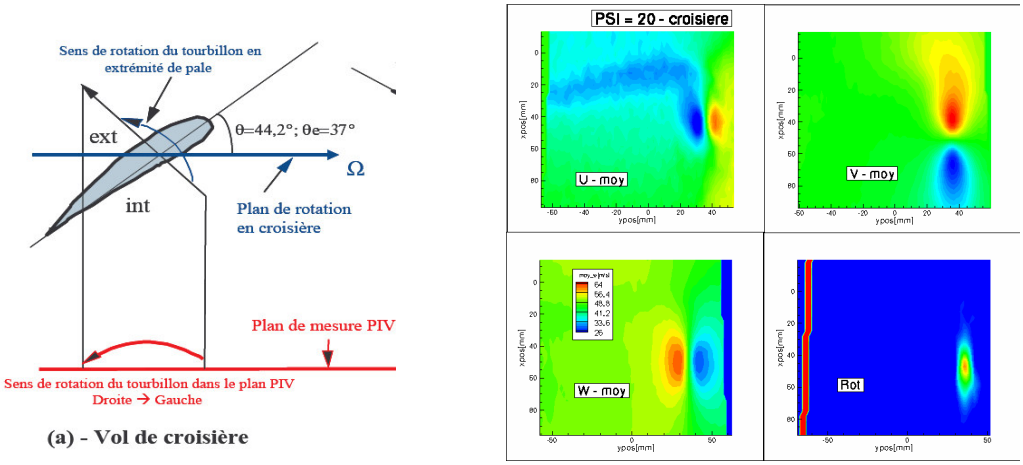

Figure 14: Tip vortex geometry (left) and speed components in P2 plane (right))

P3 plane

As stated earlier, this plane is located downstream off the wing; near the trailing edge and aim at observing the vortices distortion produces by the wake interactions with the wing.
On Figure 15 (left) is plotted the location and intensity of the tip vortices "captured" by P3 plane in function of the blade azimuth. One can notice that the vortices are still regularly disposed in function of azimuth, except in the wing trailing edge area where the vortex identification is difficult using only the vorticity magnitude. In addition, due to diffusion, the vortices intensity has been reduced between P2 and P3 plane. Figure 15 (right) provide the vortices location for azimuths around wing interaction. It seems that, just above the wing, in the trailing edge region, 2 vortices can be observed.

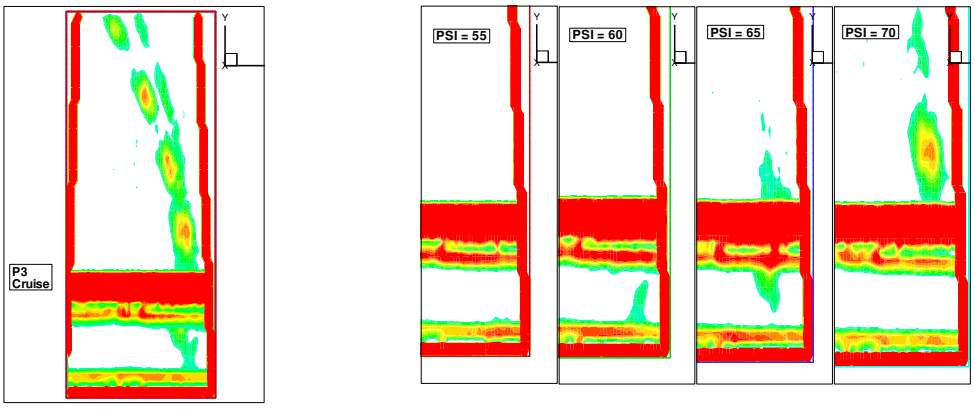

Figure 15: Location of tip vortices in P3 plane (left) and zoom on wing / vortex interaction (right))

In order to check this assumption, in Figure 16 are plotted the V component values (positive along the wingspan) for various azimuthal positions. As a reference, in the left side of the figure is recalled the V component distribution for the P2 plane. For azimuth 55 and 60 °(below the wing), the V component distribution is similar to cruise conditions but with reduced intensity. Between 65 and 75°, when the observed vortices have been interacting with the wing, this distribution is modified. Actually, at 65°, the vortex that has been interacting with the wing leading edge, results in only the lower negative transversal speed, below the wing. The increased intensity and dimension of the negative V speed zone at this azimuth may be attributed to the merging of the vortices below the wing. For the same azimuth, the vortex that has circulated above the wing upper side is also visible as it has been accelerated by the increase of speed above the wing. For higher azimuth, the vortex is relatively distorted with a strong reduction of the negative lower part of V which seems to be absorbed by the trailing edge negative zone.

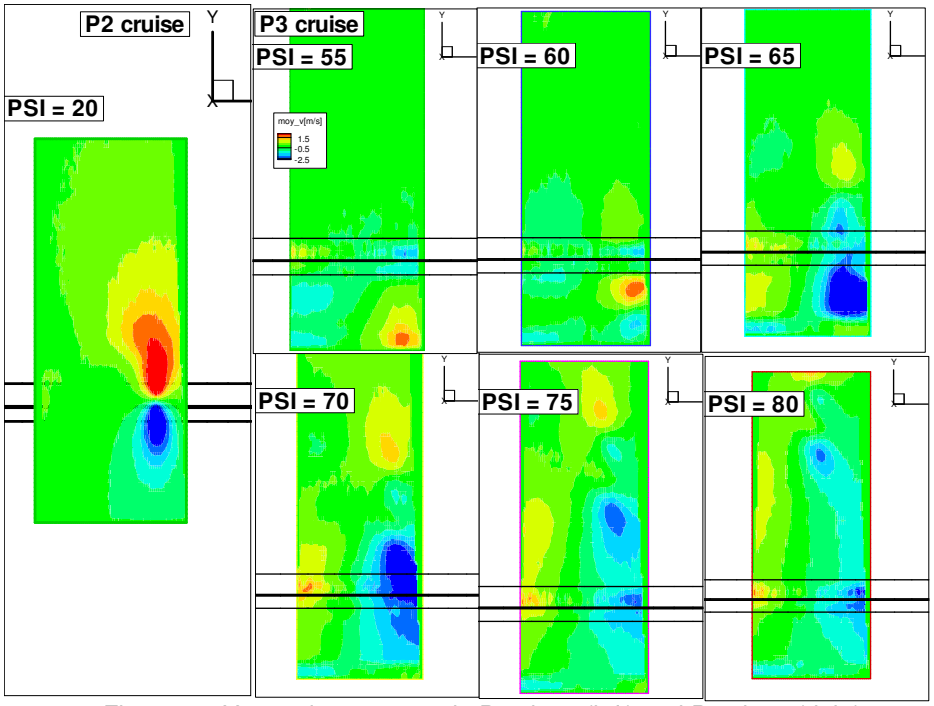

Figure 16: V speed component in P2 plane (left) and P3 plane (right)

3.2.2 PIV in conversion

P2 plane

The conversion configuration (β=45°) is slightly more complex to analyze due to the nacelle angle and the lower μ ratio (advancing speed / tip speed). For example, it takes 2.44 ms for the blade to rotate by 20°, but the blade tip displacement in free stream direction will vary between 0 (from 80 to 100°) up to 172 mm (from –10° + 10°). During the same period of time, the vortex only moves of 73.3 mm in direction of PIV plane: therefore; contrary to cruise conditions, the youngest vortices will pass though the PIV plane first and will not be regularly disposed.

Figure 17 (left) presents the location and intensity of the blade tip vortices going through P2 plane. The preliminary remark is confirmed by the figure with vortices impacting the plane on the opposite sense of rotation of the blade. Here also, the PIV resolution is not the same in the entire plane with a better quality in the lower side. Figure 17 (right) present a comparison of tip vortices experimental location with the theoretical ones predicted with HOST code (isolated rotor assumptions). The side

view presented on the right figure enables to visualize why the older vortices arrive latter. The front view shows the good agreement with theoretical location.

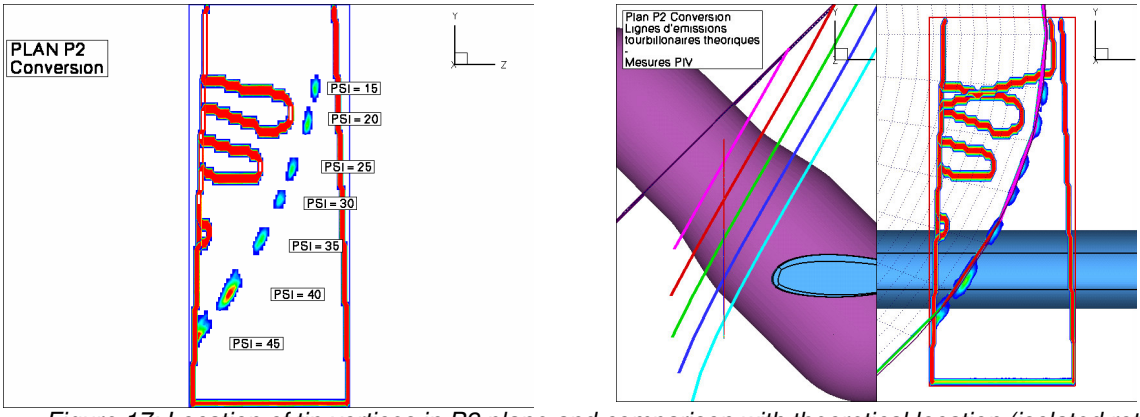

Figure 17: Location of tip vortices in P2 plane and comparison with theoretical location (isolated rotor)

Figure 18 (right) presents briefly the 3 speed components (averaged value) for 1 azimuthal blade location. Here, as plotted on the left side of the figure, the nacelle angle is 45°, the collective pitch reaches 20° for a –7° twist at blade tip, and thus the blade tip has 32° deg of angle with the PIV plane. The tip vortex is therefore tilted, its rotational vector also having a 32° deg of incidence directed downwards.

Concerning W components (free stream direction), one can check that the average speed outside wake influence reaches the expected 30 m/s and that the internal part of the tip vortices increases the speed whereas the extern part reduces it. For U component (vertical speed for the wing; negative upwards), the spatial location of the vortex is confirmed with the increase of incidence at the internal part of the vortex. The V component (along wingspan) add the last piece of information for vortex spatial location with positive value on the lower part

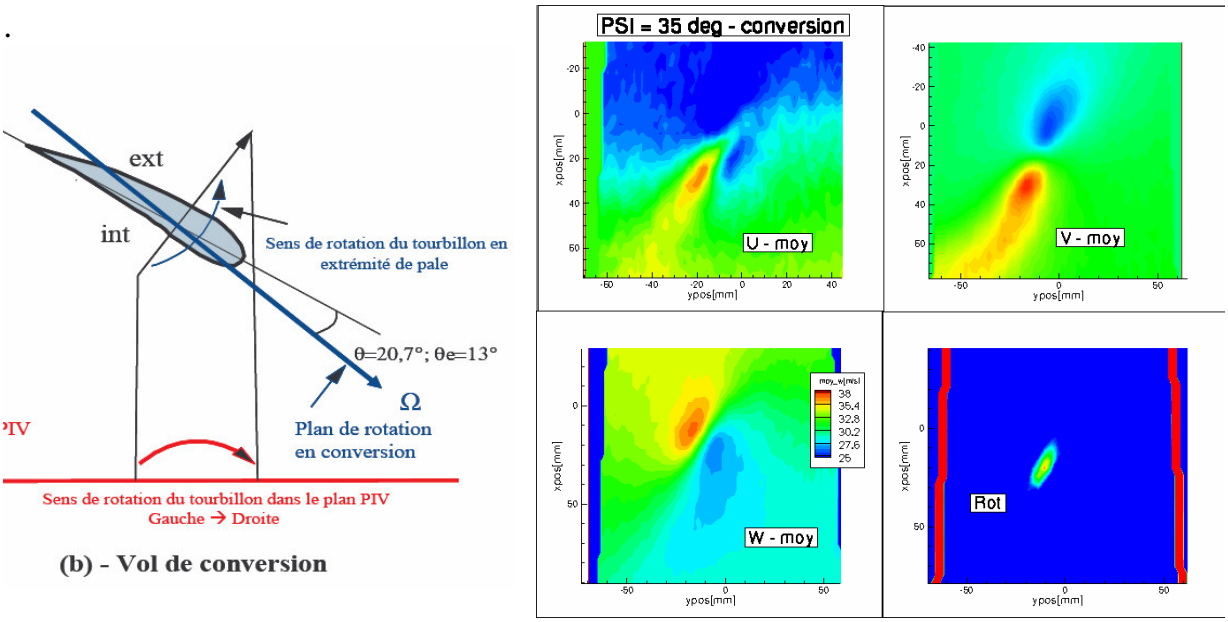

Figure 18: Tip vortex geometry (left) and speed components in P2 plane (right))

P3 plane

The P3 plane adapted on cruise configuration was also used in conversion.

On Figure 19 (left) is plotted the location and intensity of the tip vortices "captured" by P3 plane in function of the blade azimuth. The global shape of the vortices "path" is similar to cruise, except near trailing edge area, with the youngest vortices passing first through the PIV plane. Unluckily, as the latest recorded azimuth for blade 1 is 120°, we miss the vortices interacting with the lower side of the wing for the blade 1. Figure 19 (right) provide the vortices location for azimuth around wing interaction. The 120 ° vortex is quite different from the others with an opposite inclination.

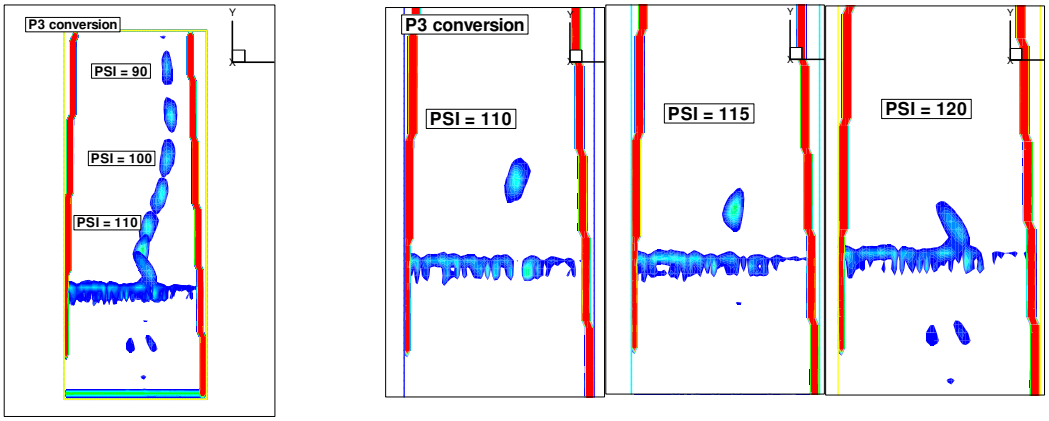

Figure 19: Location of tip vortices in P3 plane (left) and zoom on wing / vortex interaction (right)

As for cruise conditions, in Figure 20 are plotted the V component values (positive along the wingspan) for various azimuthal positions. As a reference, in the left side of the figure is recalled the V component distribution for the P2 plane. The main learning is that there is two merging vortices for all the plotted azimuths: the can be clearly observed at 110 and 115°. Moreover, contrary to cruise configuration, the lower part of the wing mostly experience a positive V speed after the rotor interactions.

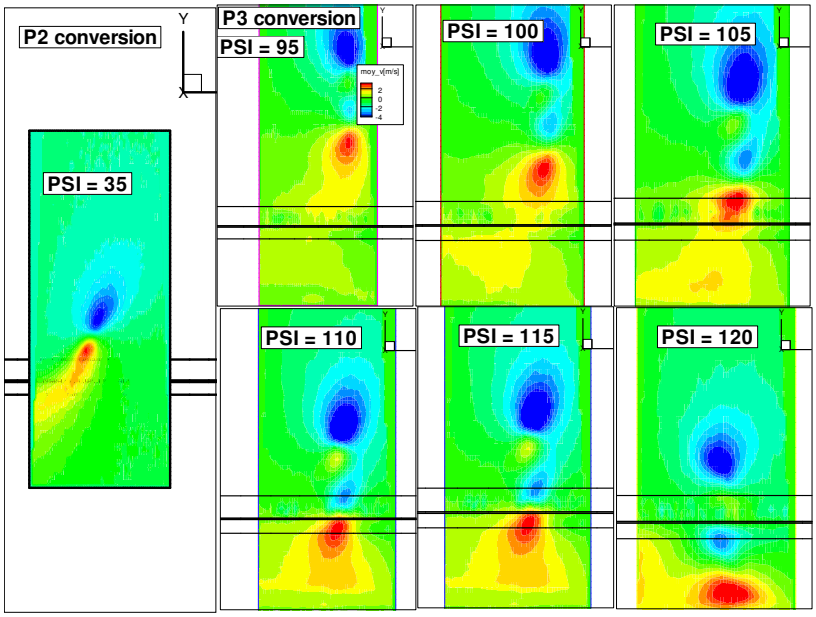

Figure 20: V speed component in P2 plane (left) and P3 plane (right)

3.3 Conclusion on PIV measurements

The 2nd year of the experimental study of aerodynamic interaction of tilt rotor in LABM was used to set up PIV 3C measurements. The analysis of the PIV planes in cruise and conversion configuration demonstrates the good capabilities of this measurement technique to analyse the vortices 3D geometry and its characteristics, even after the wing interactions. The next step will be to improve the accuracy of PIV resolution and to modify the experimental set-up to measure PIV plane above (and below) the wing in order to characterize the modifications of vortices geometries and trajectories when impinging the wing.

4. ACKNOWLEDGEMENTS

The authors would like to acknowledge the French DPAC for funding the present study.

CONCLUSION

This paper described the 2nd year of the collaborative research work between LABM and ONERA research center on the studies of aerodynamic interactions occurring on a tilt-rotor configuration.
During 1st year of studies, several experimental methods have been developed and applied to a 1/7 tilt-rotor scale model operating in different flight configurations. Data concerning the rotor performance, the wake and the wing aerodynamic behaviour have been obtained.
During the 2nd year of the research work, both numerical and experimental studies were conducted. Considering CFD calculations, the selected mesh strategy and the calculations parameters allowed to reproduce the experimental behaviour of the rotor / wing interactions measured in cruise, especially using the non uniform actuator disk hypothesis. The numerical set-up can therefore be used to improve the knowledge of the physical phenomenon occurring during the aerodynamic interactions for the transition phase, even if some improvements will have to be done (like including transition).
Considering the PIV 3C measurements, the 2nd year of the experimental study was used to set up PIV 3C measurements. The analysis of the results demonstrates the good capabilities of this measurement technique to reach the vortices 3D characteristics. The experimental set up will therefore be used to investigate the modifications of vortices geometries and trajectories when impinging the wing, especially in conversion configurations.
Finally, the combination of both numerical and experimental studies on the same WT model is very fruitful and will be used to improve numerical models of tilt-rotor wakes interactions.

REFERENCES

[1] C. Matos, U. Reddy and N.K. Komerath, “Rotor Wake/Fixed Wing Interactions with Flap Deflection”, 55th Annual Forum of AHS, Montreal, Canada, May 1999.
[2] C. Barla, T. Lefebvre, E. Berton, P. Beaumier, D. Favier “Experimental and numerical investigation of aerodynamic interaction on a tilt rotor configuration”, 32nd European Rotorcraft Forum, Maastricht, Netherlands, September 2006
[3] W. Johnson, “*Calculations of the Aerodynamic Behavior of the Tilt Rotor Aeroacoustic Model (TRAM) in the DNW*”, Proceedings of the 57th AHS Annual Forum, Washington D.C., May 1999
[4] *« Rotor wake / fixed wing interactions with Flap Deflection* », C. Matos and al., AHS, Montréal, Mai 1999
[5] *« Vortex wake geometry of a model Tilt Rotor in a forward flight* », G.K. Yamauchi and al., AHS Interantional Meeting, Tochigi (Japon), Novembre 2002

[6] *«Tilt Rotor aerodynamics phenomena in low speed forward flight* », M. A. Potsdam and al., AHS, San Francisco, Janvier 2004

[7] *"Unsteady wing surface pressures in the wake of a propeller",* R.T. Johnston and J.P. Sullivan, 30th Aerospace Sciences Meeting & Exhibit, Reno, USA, January 1992

[8] B. Benoit, J.M. Bousquet, " *Aerodynamic design of a tilt-rotor blade*", 17th ICAS Congress, Stockholm (Sweden), September 9-14, 1990

[9] *"Improvement of the robustness of Chimera method",* C. Benoit, M-C. Le Pape, G. Jeanfaivre, 32nd AIAA Fluid Dynamic Conference & Exhibit , Saint Louis, USA, June 2002

[10] *Actuator disk modeling for helicopter rotors",* F. Le Chuiton, 28th ERF, Brisotl, UK, September 2002

[11] *"elsA; an efficient object-oriented solution of CFD complexity",* L. Cambier, M. Gazaix, 40th AIAA Aerospace Scicnece meeting Exhibit, Reno, USA, January 2002

[12] *« A two-dimensionnal viscous aerodynamic design analysis Ccode »,* M. Drela and al., AIAA paper, 87-0424, 1987

[13] B. Benoit, A.-M. Dequin, K. Kampa, W. Grunhagen, P.-M. Basset, B. Gimonet, "*HOST, A General Helicopter Simulation, Tool for Germany and France*", 56th Annual Forum of the American Helicopter Society, Virginia Beach (USA), May 2002